ACS APPLIED MATERIALS & INTERFACES

Research Article

www.acsami.org

Low-Temperature Growth of Carbon Nanotube Forests Consisting of Tubes with Narrow Inner Spacing Using Co/Al/Mo Catalyst on Conductive Supports

Hisashi Sugime,*[,†] Santiago Esconjauregui,[†] Lorenzo D'Arsié,[†] Junwei Yang,[†] Alex W. Robertson,[‡] Rachel A. Oliver,[§] Sunil Bhardwaj,[∥] Cinzia Cepek,[∥] and John Robertson[†]

[†]Department of Engineering, University of Cambridge, Cambridge CB3 0FA, United Kingdom

[‡]Department of Materials, University of Oxford, Parks Road, Oxford, OX1 3PH, United Kingdom

[§]Department of Materials Science and Metallurgy, University of Cambridge, Cambridge CB3 0FS, United Kingdom

[∥]Istituto Officina dei Materiali-CNR, Laboratorio TASC, Trieste I-34149, Italy

ABSTRACT: We grow dense carbon nanotube forests at 450 °C on Cu support using Co/Al/Mo multilayer catalyst. As a partial barrier layer for the diffusion of Co into Mo, we apply very thin Al layer with the nominal thickness of 0.50 nm between Co and Mo. This Al layer plays an important role in the growth of dense CNT forests, partially preventing the Co−Mo interaction. The forests have an average height of ∼300 nm and a mass density of 1.2 g cm^{-3} with tubes exhibiting extremely narrow inner spacing. An ohmic behavior is confirmed between the forest and Cu support with the lowest resistance of ∼8 kΩ. The forest shows a high thermal effusivity of 1840 J $s^{-0.5}$ m^{-2} K^{-1}, and a thermal conductivity of 4.0 J s^{-1} m^{-1} K^{-1}, suggesting that these forests are useful for heat dissipation devices.

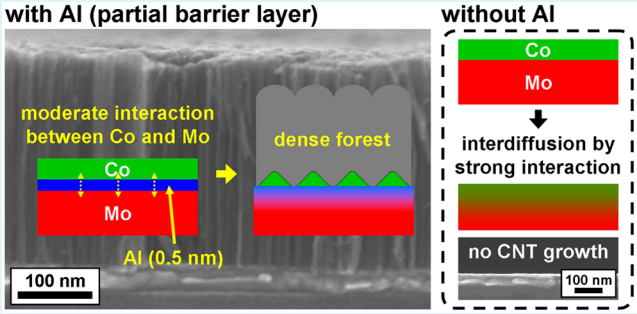

KEYWORDS: *chemical vapor deposition, low-temperature growth, thermal effusivity, thermal conductivity, sputtering, cocatalyst, catalyst nanoparticles*

1. INTRODUCTION

Owing to their outstanding mechanical, electrical, and thermal properties, carbon nanotubes (CNTs) are envisaged as the building block in wide range of industries.[1−4] For industrial applications to materialize, however, it is necessary to control the synthesis, to tailor the structure and properties, and to achieve this in an inexpensive way. From the various morphologies that can be obtained in the synthesis, vertically aligned CNT forests are the form most relevant to potential high-tech industrial applications, such as interconnects in next-generation electronics,[5,6] heat dissipation devices,[7,8] super-capacitors,[9,10] field emission devices,[11,12] or membranes.[13−15] Forests are typically synthesized by chemical vapor deposition (CVD) as it is particularly suited to industrial scale up because of the relatively low process temperature. Especially for complementary metal-oxide-semiconductor (CMOS) compatible processes, the temperature needs to be lower than 450 °C, while it is typically 700−900 °C. In order to grow CNT forests with such low temperature, we and other groups have reported the optimization of both CVD and catalyst conditions.[16−22]

Integrating as many carbon walls as possible in the limited space of CNT forests is another important issue. A larger number of carbon walls is preferred for applications because each wall behaves as an electrical or thermal channel when it is properly contacted.[23] This can be done either by reducing the space between tubes (outer spacing), or by reducing the space within each tube (inner spacing). When the tube diameter is fixed, the outer spacing can be reduced by increasing area density, which has reached as high as ∼1−2 × 10^{13} cm^{-2} to date.[24,25] The inner spacing can be reduced by increasing the wall number per tube, which is a more challenging strategy.

We focus on engineering the catalyst/support systems to integrate the large number of carbon walls in the CNT forests. Multilayer or binary catalysts, which drastically enhance the height or the density of the forest, are widely studied. Aluminum oxide layers (Al_2O_3 or Al_2O_x), typically with the thickness of 5−20 nm, are often used to obtain tall CNT forests, up to the millimeter scale, by combining them with Fe, Co, or Ni.[26−33] Mo is also used to grow CNT forests in combination with Fe or Co.[34−37] In particular, Co−Mo binary catalyst is known as the first combination that has enabled the growth of single-wall CNT (SWCNT) forests on SiO_2.[34] It is suggested that Co and Mo form a complex carbide or oxide, which enables the Co to form small catalyst nanoparticles.[38,39] Recently, using a Co−Mo catalyst, we have achieved the growth of CNT forests on Ti-coated Cu supports at 450 °C with the

Received: June 2, 2015
Accepted: July 15, 2015
Published: July 15, 2015

DOI: 10.1021/acsami.5b04846
ACS Appl. Mater. Interfaces 2015, 7, 16819−16827

highest mass density of 1.6 g cm^{-3}.[20,21] X-ray photoelectron spectroscopy (XPS) shows that the Co−Mo−Ti interaction prevents Co nanoparticles from sintering, an effect that plays an important role for the root growth mechanism.

In this work, to extend the concept of multilayer catalyst systems and the possibility of a Co−Mo interaction, we apply a "partial barrier layer" with a very thin Al deposition between Co and Mo. In the case of forest growth on Cu supports, Ta, Ti, or TiN diffusion barrier layers are often used to completely passivate the Cu surface, thus preventing the diffusion of Fe or Co into Cu.[18,40,41] On the other hand, the thin Al layer herein allows moderate interaction between Co and Mo, partially preventing the diffusion of Co into Mo. We obtain dense CNT forests consisting of tubes with extremely narrow inner spacing that grow by the base growth mechanism. This new concept of a multilayer catalyst system with a partial barrier layer will widen the possibility to design and engineer the catalyst/support systems for the growth of CNT forests.

2. EXPERIMENTAL SECTION

2.1. Catalyst Preparation and CNT Forest Growth. We first deposit 40 nm Cu as a conductive support followed by 5.0 nm Mo on a SiO_2(200 nm)/Si(100) substrate. Then, we deposit 0.25, 0.50, or 1.0 nm Al followed by 2.5 nm Co. As reference, we also prepare samples without Al and/or Mo. All metal depositions are carried out by DC magnetron sputtering in 3.5×10^{-3} mbar of Ar. The base pressure of the chamber is below 5.0×10^{-5} mbar. All samples are exposed to air after each deposition. Subsequently, the samples are loaded in a cold-wall CVD chamber and pumped down to a base pressure of 6.0×10^{-2} mbar. We then set a nominal pressure of 3 mbar with 200 sccm NH_3 and heat the samples to 450 °C at a rate of 3 °C s^{-1} (pretreatment). Once the samples reach 450 °C, we replace the NH_3 with 200 sccm C_2H_2 to grow CNTs for 3 min. After the growth, the heater is turned off, and C_2H_2 is switched to Ar until the samples cool to room temperature.

2.2. Sample Characterization. Before the growth of CNTs, we observe the formation of Co nanoparticles on the substrates by scanning electron microscopy (SEM, Hitachi S-5500). The roughness of sample surface is measured by atomic force microscopy (AFM, Veeco Dimension 3100) in tapping mode. The images are leveled to remove a background tilt. The chemical state of metal films both after deposition and after annealing is assessed by XPS. The annealing condition is 450 °C under H_2 at 5×10^{-7} mbar for 10 min. The measurement after annealing is carried out without exposing the samples to air to avoid oxidation. Photoemission spectra are acquired at room temperature in normal emission geometry using a hemispherical electron energy analyzer and a conventional Mg $K\alpha_{1,2}$ (1253.6 eV) X-ray source, with an overall experimental energy resolution of ∼0.8 eV. The binding energy is calibrated by fixing the C 1*s* signal coming from ambient contaminants to 284.6 eV. All the spectra are normalized to the incident photon flux and analyzed by performing a nonlinear mean square fit of the data in the binding energy range of interest following the Levenberg−Marquardt algorithm. We use a Shirley background and reproduce the photoemission lineshapes of the Co 2p and Mo 3d levels using asymmetric Doniach−Sunjic curves. The Co 2p levels are reproduced using different doublets, corresponding to Co^0 ($2p_{3/2}$ at 778.4 eV, $2p_{1/2}$ at 793.4 eV, no satellite), Co^{2+} ($2p_{3/2}$ at 780.9 eV, $2p_{1/2}$ at 796.5 eV, satellites at 5.6 eV above the photo line) and Co^{3+} ($2p_{3/2}$ at 783.4 eV, $2p_{1/2}$ at 798.4 eV).[42] The Mo 3d levels are reproduced using different doublets corresponding to Mo^0 ($3d_{5/2}$ at 228.0 eV, $3d_{3/2}$ at 231.1 eV), Mo^{4+} ($3d_{5/2}$ at 228.4 eV, $3d_{3/2}$ at 231.9 eV) and Mo^{6+} ($3d_{5/2}$ at 233.0 eV, $3d_{3/2}$ at 236.1 eV).[43] The depth profiles of substrate are analyzed by time-of-flight secondary ion mass spectroscopy (TOF-SIMS, ION-TOF TOF.SIMS 5). We use a Bi liquid metal gun and a Cs ion gun. Bi ions are filtered for Bi_1^+ ions and Cs ions are filtered for Cs^+ ions. The sputtering raster is 300×300 μm^2 using Cs^+ at 500 eV (current 30 nA) and surface spectra are taken from an area of 50×50 μm^2 using Bi_1^+ at 25 keV (target current 1 pA). The guns are operated in high current bunched mode, the extractor is in positive mode, and the analyzer is optimized for high mass resolution, acquiring over a range from 0.5 to 740 Da. The depth of the crater is measured using an optical profiling system (Wyko NT1100); a constant sputtering rate is assumed throughout.

After the growth of CNTs, the samples are observed by SEM and transmission electron microscopy (TEM, JEOL 2200MCO at 80 kV, and FEI Tecnai F20 at 120 kV). The filling factor of the CNT forest is obtained from the top-view SEM images by dividing the area of the CNTs by the total area of the substrates. For TEM observation, the samples are transferred to Cu microgrids by scratching the CNT forests on the substrates. We acquire Raman spectra shining a 457 nm laser on top of the forest at ∼500 μW with a 50× objective and a spot diameter of ∼1.5 μm (inVia Renishaw microscope).

2.3. Forest Density Measurement. We weigh the Si substrates (1.5−4.0 cm^2) before and after CVD process by a microbalance (Satorius ME235S; readability, 0.01 mg). The typical weight gain of the samples by CNT forest is 0.02−0.20 mg. The volume of the CNT forests is calculated from the area of the Si substrates and the height of CNT forests. The mass density is calculated from the weight gain of the Si substrates divided by the volume of CNT forests. We obtain the area density from the mass density and the unit mass of tubes. The unit mass of tubes is obtained from the tube diameter and the wall number, which are observed by TEM.

2.4. Electrical and Thermal Properties Measurement. We measure *I*−*V* characteristics of the CNT forests by conductive AFM (Veeco Dimension 3100 equipped with a Nanoscope V controller). The setup is the same as previously reported.[44] Thermal effusivity is obtained by the picosecond thermoreflectance measurement system (PicoTherm).[45] We deposited 100 nm Mo on top of the CNT forest to get higher reflectivity from the top surface of the samples. The thermal conductivity is calculated with the thermal effusivity and the specific heat capacity of graphite (0.71 J g^{-1} K^{-1}). The relationship between the thermal effusivity and thermal conductivity is expressed as

$$b = \sqrt{\lambda c \rho} \tag{1}$$

where b, λ, c, and ρ are thermal effusivity (J $s^{-0.5}$ m^{-2} K^{-1}), thermal conductivity (J s^{-1} m^{-1} K^{-1}), specific heat capacity (J g^{-1} K^{-1}), and mass density (g cm^{-3}), respectively.

3. RESULTS

Figure 1a shows a side-view SEM image of the substrates after the CVD process. The catalyst structure is shown with a schematic in Figure 1b. The CNT forests grow with the height of ∼300 nm, and the mass density of 1.2 g cm^{-3}. Although C_2H_2 is highly reactive,[46−48] the catalyst nanoparticles are not poisoned even with the high concentration of C_2H_2 used herein (100% C_2H_2). This is because the formation of byproduct such as amorphous carbon is suppressed at relatively low growth temperature and pressure (450 °C and 3 mbar). As discussed later in detail, 0.50 nm is the optimum thickness for the Al layer, which balances the forest height and density. The forest morphology without measurable spacing between tubes (bottom inset in Figure 1a) is completely different from conventional CNT forests. From the top-view image (top inset in Figure 1a), the filling factor of the CNTs is estimated as ∼90%, indicating a very packed morphology for the as-grown forests (without any post processes). The mass density is more than double that of conventional SWCNT forests after densification by liquid (0.57 g cm^{-3}).[10] The forest and Cu support shows an ohmic behavior with the resistance of 35 ± 26 kΩ (mean ± standard deviation), which indicates the forests have good electrical contact with the conductive support. The lowest measured resistance is ∼8 kΩ, which is better than our

DOI: 10.1021/acsami.5b04846
ACS Appl. Mater. Interfaces 2015, 7, 16819−16827

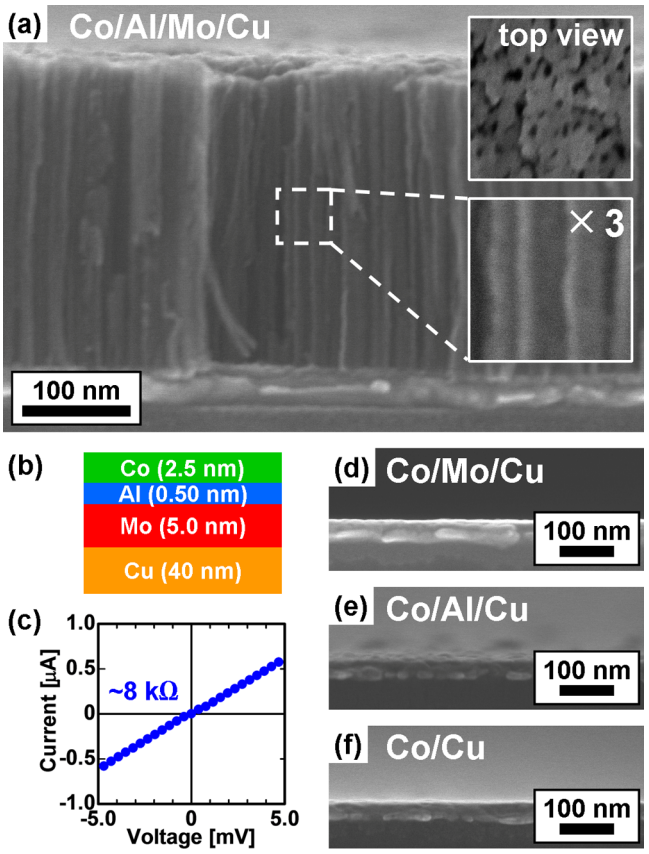

Figure 1. (a) SEM images of the samples with Co/Al/Mo on Cu support after the CVD process. (b) A schematic of the catalyst structure in panel a. (c) A typical $I-V$ curve of the CNT forest by conductive AFM. (d–f) SEM images of the reference samples with different catalyst structures (no CNT growth).

previous result by Co–Mo cocatalyst on Ti-coated Cu, Figure 1c.[20] As reference, we make the samples without Al, Mo, or both and confirm that the CNT forest grows only when both Al (0.50 nm) and Mo (5.0 nm) are present between Co and Cu (Figure 1d–f). The reason Co–Mo does not grow the CNT forests (Figure 1d) is that Mo herein (5.0 nm) is much thicker than that used in our previous work (0.8 nm).[20] The detailed mechanism is discussed later. We note that no measurable weight gain is obtained without Co (catalyst) proving that Al, Mo, and Cu do not catalyze CNT growth under the CVD condition used here.

We then characterize the tube structure in detail by TEM and Raman. The diameter distribution of individual tubes appears to be wide, ranging from 4 to 35 nm, with the diameter of 23 ± 10 nm (mean ± standard deviation). The well-graphitized structures with the lattice spacing of ~0.34 nm are observed (inset in Figure 2a). The Raman spectrum taken from the top of the forest shows G-peak (~1590 cm^{-1}) and D-peak (~1370 cm^{-1}) which is a typical spectrum for the multiwall CNTs (MWCNTs), Figure 2b. The intensity ratio of G-peak to D-peak (I_G/I_D) is 1.1, which is slightly higher than that of our previous CNT forest by Co–Mo cocatalyst (I_G/I_D = 1.0).[20] Some tubes show inner spacing with ~2 nm (as indicated by the arrows in Figure 2a), while the others show no inner spacing (Figure 2c,e–g). The average wall number is estimated to be 31, assuming that the tubes with no measurable inner spacing are filled with carbon walls. Combining the wall number with the mass density (1.2 g cm^{-3}) and the average tube diameter (23 nm), we obtain an area density of 1.3×10^{11} cm^{-2} and a wall density of 4.1×10^{12} cm^{-2}, respectively. We observe most of the catalyst particles at the bottom of the tubes (arrow indication in Figure 2d,g). This is the clear indication that the Co nanoparticles interact strongly with the support (Al/Mo/Cu) resulting in the base growth mechanism. The catalyst particles, with diameter as great as 15 nm, do not have a spherical shape but a deformed one due to the presence of carbon wall of CNTs (as indicated by the arrows in Figure 2d).

It is found that both Al (0.50 nm) and Mo (5.0 nm) are necessary for dense CNT forest growth (Figure 1). We characterize the formation of Co catalyst nanoparticles under different catalyst conditions. Figure 3 shows the top-view SEM and AFM images of the sample surfaces after the pretreatment at 450 °C under NH_3 (before flowing C_2H_2). With Co/Al/Mo on Cu support, where the CNT forest grows, Co forms nanoparticles with diameters of 9.8 ± 3.0 nm (mean ± standard deviation) and area density of 1.8×10^{11} cm^{-2}, Figure 3a. The root-mean-square roughness (R_q) is 1.5 nm, indicating the formation of nanoparticles (Figure 3b). Combining the area density of Co nanoparticles with the area density of the tubes (1.3×10^{11} cm^{-2}), ~75% of Co nanoparticles are found to be catalytically active. On the other hand, Co does not form nanoparticles with Co/Mo/Cu (R_q = 0.44 nm, Figure 3c,d), Co/Al/Cu (R_q = 0.51 nm, Figure 3e,f), and Co/Cu (R_q = 0.78 nm, Figure 3g,h). This is the reason the CNT forests do not grow on the samples. The results are consistent with the fact that the formation of catalyst nanoparticles is suppressed on conductive supports by their high surface energy.[49−51]

We then investigate the role of a thin Al layer (0.50 nm) by measuring the depth profile of the samples by SIMS. We compare the samples with and without Al after a pretreatment at 450 °C in NH_3. We observe clear interfaces between the metal layers when the Al layer is present, Figure 4a. The interfaces of Co/Al/Mo and Mo/Cu are at ~3 and ~9 nm respectively, where the intensity of each metal decreases by the same ratio from the maximum intensity. This is largely in agreement with the original heterostructure used. The slight spread of the peaks is due to measurement artifacts such as beam-induced mixing and slight tilt of the sample during measurement. When the Al layer is absent, there are no clear interfaces between the Co, Mo, and Cu layers (Figure 4b), suggesting the interdiffusion between the metal layers. We observe both Co and Mo diffusion into the Cu bulk as well as backward diffusion of Cu toward the surface of the sample. The thin Al layer, even with a thickness of 0.50 nm, clearly prevents the diffusion of Co into Mo layer.

To further assess the effect of Al layer on the catalyst system, we perform XPS characterization on samples with and without Al, both before and after annealing under H_2, Figure 5. As the samples are not exposed to air after annealing, we can exclude the possible oxidation. Before H_2 annealing, in both substrates (with and without Al), the Co 2p has the typical line shape of Co^{2+} (yellow component), with a possibly small amount of Co^{3+} (green component),[42] while the Mo 3d is found to be mainly in a metallic state, with possibly a very small contribution of Mo^{4+}.[43] We note that Al 2p peak is overlapped with Co 3p peak and is too small to be observed. The presence of Al enhances the reducing effect of H_2 annealing in Co. When Al is present, the intensity of Co^0 peak (red component), present in both cases, is ~30% higher, and it is the dominating component. It is well-known that the Co–Al system is characterized by a strong interaction, where Co is partially

DOI: 10.1021/acsami.5b04846
ACS Appl. Mater. Interfaces 2015, 7, 16819−16827

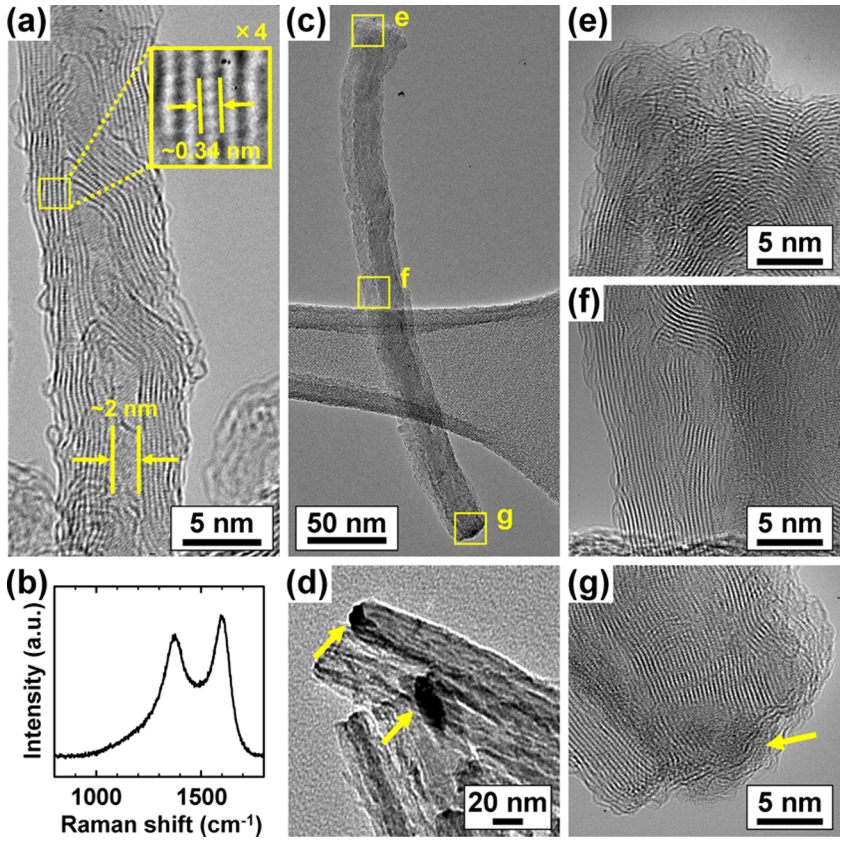

Figure 2. (a and c–g) TEM images and (b) Raman spectra of the CNT forests grown by Co/Al/Mo catalyst on Cu support. Panels e, f, and g are the enlarged images of the areas shown with squares in panel c, respectively.

reduced even if the system is annealed in a non-reducing atmosphere.[52] This is possibly because Al extracts the oxygen atom from Co by a larger affinity to oxygen (Al_2O_3: $\Delta_f G^o$ = −1582.3 kJ mol^{-1}).[53] The same mechanism has been reported with Fe–Ta catalyst as the solid-state reduction.[54,55] The annealing in the presence of a reduction gas, as H_2, NH_3, or both, enhances the fraction of metallic Co, which is active state to grow CNTs. A similar behavior is also found in the analysis of the Mo 3d level. Before annealing, Mo is found on both substrates in its metallic state, which does not change in the presence of Al. After annealing, more oxidized states with Mo^{4+} or Mo^{6+} are observed when Al is absent.

4. DISCUSSION

4.1. Role of Thin Al Layer and Growth Mechanism of Tubes with Narrow Inner Spacing. It is found that 0.50 nm Al plays an important role in the growth of the dense CNT forests, although it is much thinner than the other metals (Co, Mo, and Cu). As shown by the SEM images and schematics in Figure 6, the forest morphology largely depends on Al thickness. The forest height decreases roughly by half with 0.25 nm Al (left images in Figure 6a), while the area density of the forest significantly decreases with 1.0 nm Al (right images in Figure 6a). From these growth results, we conclude that 0.50 nm is the optimum thickness to balance the forest height and density. We have previously shown that CNT forests do not grow with 2.5 nm Co on Mo layers thicker than ∼1 nm,[21] and XPS measurements have shown that Co and Mo interact strongly during the CVD process.[20] This strong interaction causes the interdiffusion of Co and Mo, thus hindering the formation of Co nanoparticles and forest growth (Figures 1d, 3c,d, 4b, and 6b). This is in agreement with the fact that the forest growth on conductive supports is more challenging than that on insulating supports.[56,57] The same mechanism can explain the Co/Cu case (without Al and Mo, Figure 1f, 3g,h, and 6c). The 0.50 nm Al layer, which is oxidized by air exposure, partially prevents the Co–Mo interaction. This helps the formation of Co nanoparticles with area density of 1.8 × 10^{11} cm^{-2} (Figure 3a,b), and with more metallic state (Figure 5).

The forest height decreases with thinner Al (e.g., 0.25 nm), as shown in the left images in Figure 6a. The addition of Al layer lessens the interaction between Co and Mo. However, as 0.25 nm is not optimum, Co and Mo partially interdiffuse, resulting in the lack of active Co nanoparticles. On the other hand, when the Al layer is too thick (e.g., 1.0 nm), the forests grow with low area density because the Co–Mo interaction becomes too weak (right images in Figure 6a). The weak interaction is not sufficient to prevent Co nanoparticles from sintering or being lifted off the substrates. As shown in the schematics on the right images of Figure 6a, we observe by TEM that some Co particles lifted off from the substrates and embedded in the tip or the middle of the tubes (data not shown). We observe the lift-off of Co nanoparticles also in the forest growth by Co–Mo on Ti-coated Cu, when Mo becomes too thin (or without Mo), resulting in the weak interaction between Co and supports.[20,21] Although the surface energy of Cu (1.56 J m^{-2}) is smaller than that of Mo (2.51 J m^{-2}),[58] the forests do not grow with Co/Al/Cu (without Mo, Figure 1e, 3e,f, and 6d). This is possibly because Co does not form a complex carbide or oxide with Cu unlike Co–Mo.[38,39]

DOI: 10.1021/acsami.5b04846
ACS Appl. Mater. Interfaces 2015, 7, 16819–16827

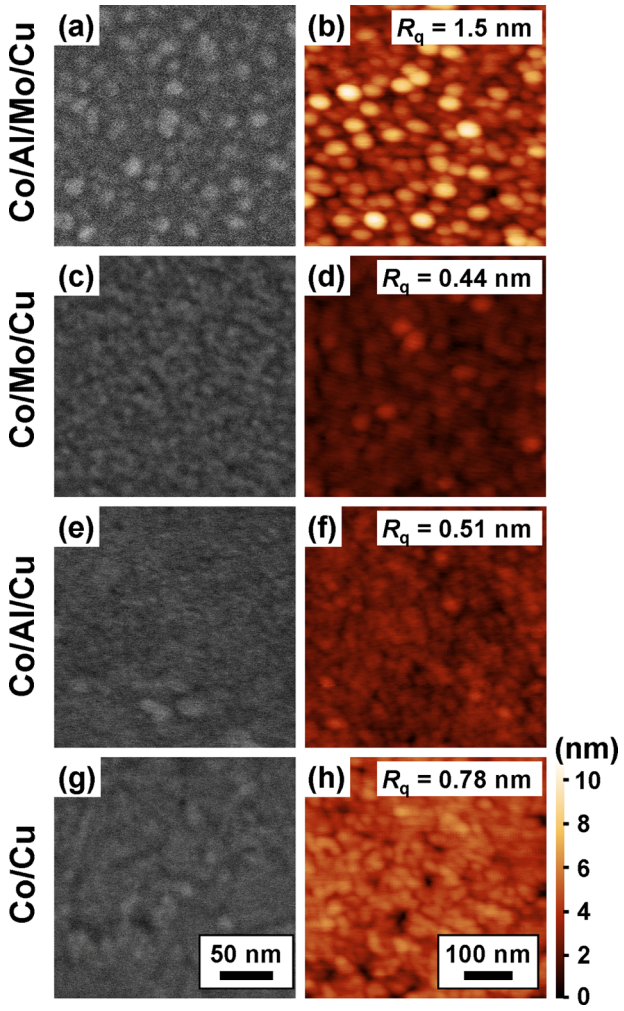

Figure 3. Top-view (a, c, e, and g) SEM and (b, d, f, and h) AFM images of the sample surfaces with different catalyst conditions after the pretreatment at 450 °C in NH_3. The scale bars in SEM and AFM images are the same for all the images.

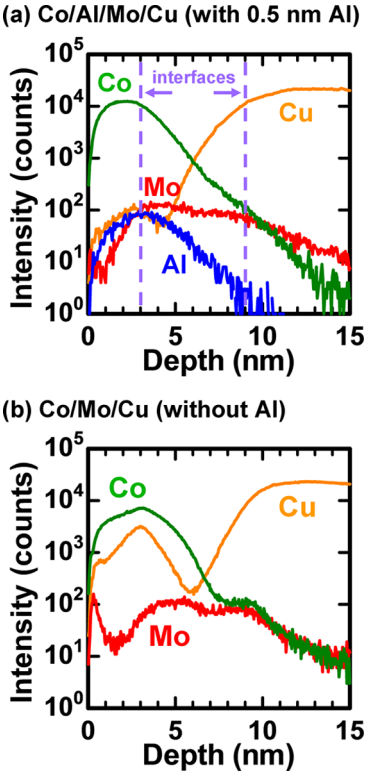

Figure 4. Depth profiles of the samples (a) with and (b) without Al after annealing at 450 °C under NH_3.

4.2. Relationship between Area Density, Wall Density, and Mass Density of CNT Forests. In the case of conventional tubes, the tube diameter is correlated to the dimensions of the catalyst particles, that is, the particles display a spherical shape, and the tube diameter matches the catalyst diameter. However, most Co nanoparticles herein show a deformed shape, as observed by TEM (Figure 2). At high temperatures (700−900 °C), the typical optimum Co thickness for tall SWCNT forests is ∼0.2 nm with Mo on SiO_2[59] and ∼0.7 nm on aluminum oxide (Al_2O_3 or Al_2O_x).[33] The Co layer herein is 2.5 nm which is more than ∼3 times thicker than that of Co thicknesses mentioned above, thus forming larger particles of up to ∼15 nm (from TEM and SEM, Figures 2d and 3a). During the growth, these large Co particles are deformed by a strong interaction both with supports and carbon walls to minimize the surface energy.[60] These deformed Co nanoparticles possibly contribute to the growth of tubes with extremely narrow inner spacing.

To maximize the number of carbon walls per unit area in a forest, we must reduce either the spacing between tubes (outer spacing) or the spacing within each tube (inner spacing). When the tube diameter is fixed, the outer spacing can be reduced by increasing area density, while the inner spacing can be reduced by increasing wall number per tube. The area density and the mass density are in a trade-off relationship when the wall density is fixed.

For example, the CNT forest consisting of 31 walls MWCNTs with the diameter of 23 nm (average values in this work, Figure 7a), and the one consisting of SWCNTs with the diameter of 2.0 nm (Figure 7b) have the same wall density of 4.1×10^{12} cm^{-2}. The latter SWCNT forest is an extreme example, and the distance between tubes is intentionally set to 5.3 nm. The MWCNT forest in Figure 7a has mass density of 1.2 g cm^{-3}, which is ∼6 times higher than that of the SWCNT forest in Figure 7b (0.19 g cm^{-3}). This means that we can integrate more carbon walls into the limited space of CNT forests. The MWCNT forest with relatively large diameter can be applied in heat dissipation devices. On the other hand, SWCNT (or few-wall CNT) forest with small diameter can be used as electrical conduction channels, since each tube has more uniform quantum resistance. By optimizing the catalyst thickness and growth condition, we are successful in growing the forest that fills the unused spacing in each tube. The tubes in this work have an extremely small ratio of the inner spacing to the tube diameter compared to the conventional tubes, Figure 7c. The values for the conventional tubes are calculated based on the paper reported by Chiodarelli et al.[61] This narrow inner spacing possibly comes from the deformed catalyst particles, as mentioned in section 4.1.

4.3. Thermal Properties of the CNT Forests. Finally, the thermal property of the CNT forest is obtained by the picosecond thermoreflectance measurement system.[45] The results are summarized in Table 1 and are compared with our previous CNT forest grown with Co−Mo catalyst on Ti-coated Cu.[20] The forest in this work shows a thermal effusivity of 1840 J $s^{-0.5}$ m^{-2} K^{-1} and thermal conductivity of 4.0 J s^{-1}

DOI: 10.1021/acsami.5b04846
ACS Appl. Mater. Interfaces 2015, 7, 16819−16827

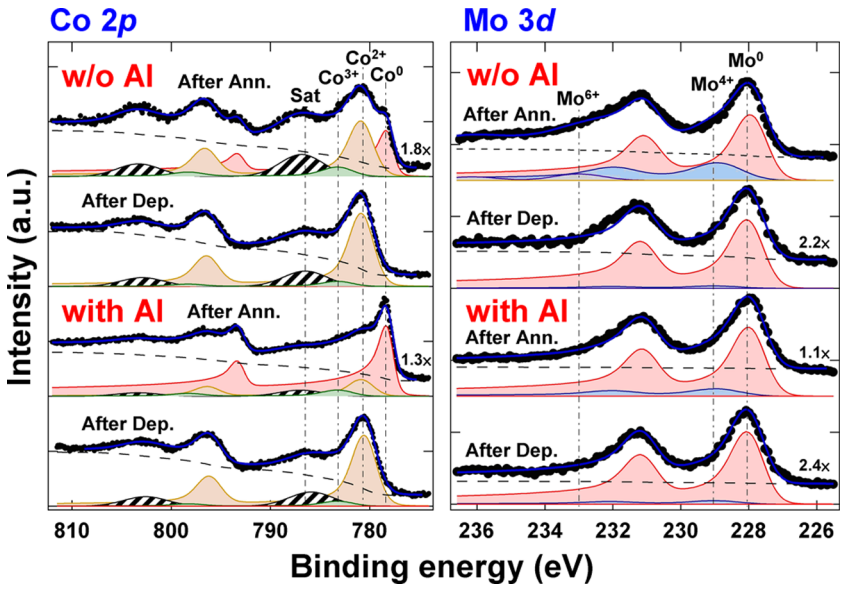

Figure 5. XPS spectra (Co 2p and Mo 3d) of the samples with and without Al, and before (after deposition) and after annealing at 450 °C for 10 min. The atmosphere during the annealing is H_2 at 5×10^{-7} mbar.

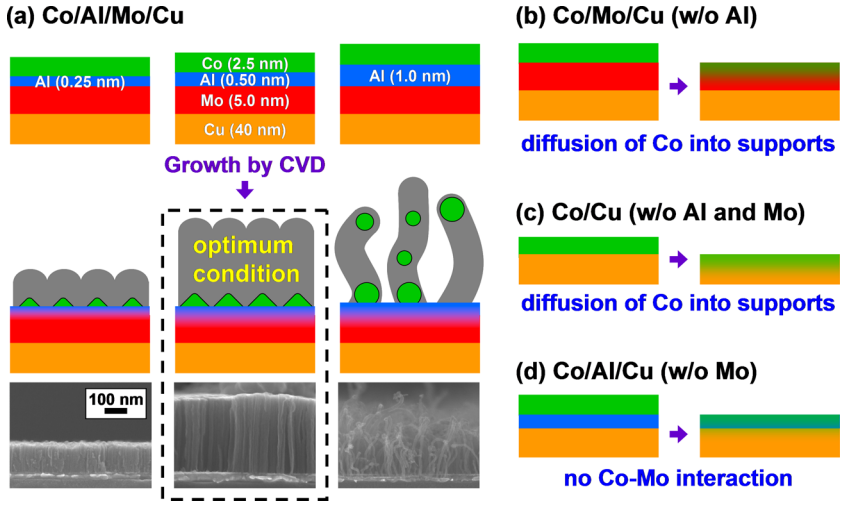

Figure 6. (a–d) Schematics and SEM images of the growth mechanism of the CNT forests by Co/Al/Mo catalyst on Cu support. The scale bar is the same for all the SEM images.

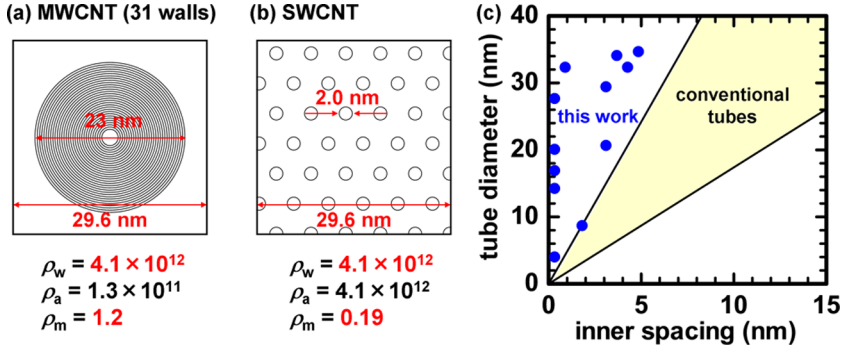

Figure 7. Schematics and summarized properties of CNT forests with (a) 31 walls MWCNTs (diameter, 23 nm), and (b) SWCNTs (diameter, 2.0 nm). ρ_w, ρ_a, and ρ_m are wall density (cm^{-2}), area density (cm^{-2}), and mass density (g cm^{-3}), respectively. The rectangle in panel a shows a unit area of the corresponding tube in the forest (~760 nm^2). (c) Relationship between inner spacing and tube diameter, comparing the tubes in this work with conventional tubes. The data for conventional tubes is based on a paper reported by Chiodarelli et al.[61]

m^{-1} K^{-1}. These values are ~2 and ~4 times higher than that reported with as-grown dense vertical graphene layers (975 J $s^{-0.5}$ m^{-2} K^{-1}, and 1.0 J s^{-1} m^{-1} K^{-1}),[45] suggesting that the forests are useful for heat dissipation devices. The forest herein

DOI: 10.1021/acsami.5b04846
ACS Appl. Mater. Interfaces 2015, 7, 16819–16827

Table 1. Thermal Properties of CNT Forests Grown with Co/Al/Mo Catalyst on Cu Support and with Co/Mo/Ti Catalyst on Cu Support[20]

	Co/Al/Mo/Cu (this work)	Co/Mo/Ti/Cu (ref 20)
thermal effusivity ($J\ s^{-0.5}\ m^{-2}\ K^{-1}$)	1840	2100
thermal conductivity ($J\ s^{-1}\ m^{-1}\ K^{-1}$)	4.0	3.9

does not have horizontal graphene layers, which prevent the heat conduction in the vertical direction, on top of the forest. This is the reason our forest shows a high thermal effusivity even with as-grown samples.

5. CONCLUSION

We grow carbon nanotube forests at 450 °C on Cu support using a Co/Al/Mo multilayer catalyst system. The forests have a height of ∼300 nm and a mass density of 1.2 g cm^{-3}. The forests consist of tubes with ∼30 carbon walls and extremely narrow inner spacing. The 0.50 nm Al layer plays an important role as a partial barrier layer that prevents the interdiffusion between Co and Mo but allows a moderate Co−Mo interaction. Due to the Co−Mo interaction, Co forms nanoparticles with high area density, and the CNT forest grows with the base growth mechanism. An ohmic behavior is confirmed between the forest and Cu support with the lowest resistance of ∼8 kΩ. The forest exhibits a high thermal effusivity of 1840 $J\ s^{-0.5}\ m^{-2}\ K^{-1}$ and a thermal conductivity of 4.0 $J\ s^{-1}\ m^{-1}\ K^{-1}$, suggesting that these forests are useful for heat dissipation devices.

AUTHOR INFORMATION

Corresponding Author

*E-mail: hs521@cam.ac.uk.

Notes

The authors declare no competing financial interest.

ACKNOWLEDGMENTS

This work has been funded by the European projects Technotubes and Grafol. H.S. acknowledges a research fellowship from the Japanese Society for the Promotion of Science (JSPS). The European Research Council has provided financial support for R.A.O. under the European Community's Seventh Framework Programme (FP7/2007-2013)/ERC grant agreement no. 279361 (MACONS).

REFERENCES

(1) Yao, Z.; Kane, C. L.; Dekker, C. High-Field Electrical Transport in Single-Wall Carbon Nanotubes. *Phys. Rev. Lett.* **2000**, *84*, 2941−2944.

(2) Berber, S.; Kwon, Y. K.; Tomanek, D. Unusually High Thermal Conductivity of Carbon Nanotubes. *Phys. Rev. Lett.* **2000**, *84*, 4613−4616.

(3) Kim, P.; Shi, L.; Majumdar, A.; McEuen, P. L. Thermal Transport Measurements of Individual Multiwalled Nanotubes. *Phys. Rev. Lett.* **2001**, *87*, 215502.

(4) Park, J. Y.; Rosenblatt, S.; Yaish, Y.; Sazonova, V.; Ustunel, H.; Braig, S.; Arias, T. A.; Brouwer, P. W.; McEuen, P. L. Electron-Phonon Scattering in Metallic Single-Walled Carbon Nanotubes. *Nano Lett.* **2004**, *4*, 517−520.

(5) Kreupl, F.; Graham, A. P.; Duesberg, G. S.; Steinhogl, W.; Liebau, M.; Unger, E.; Honlein, W. Carbon Nanotubes in Interconnect Applications. *Microelectron. Eng.* **2002**, *64*, 399−408.

(6) Naeemi, A.; Meindl, J. D. Compact Physical Models for Multiwall Carbon-Nanotube Interconnects. *IEEE Electron Device Lett.* **2006**, *27*, 338−340.

(7) Ngo, Q.; Cruden, B. A.; Cassell, A. M.; Sims, G.; Meyyappan, M.; Li, J.; Yang, C. Y. Thermal Interface Properties of Cu-Filled Vertically Aligned Carbon Nanofiber Arrays. *Nano Lett.* **2004**, *4*, 2403−2407.

(8) Huang, H.; Liu, C. H.; Wu, Y.; Fan, S. S. Aligned Carbon Nanotube Composite Films for Thermal Management. *Adv. Mater.* **2005**, *17*, 1652−1656.

(9) Du, C. S.; Yeh, J.; Pan, N. High Power Density Supercapacitors Using Locally Aligned Carbon Nanotube Electrodes. *Nanotechnology* **2005**, *16*, 350−353.

(10) Futaba, D. N.; Hata, K.; Yamada, T.; Hiraoka, T.; Hayamizu, Y.; Kakudate, Y.; Tanaike, O.; Hatori, H.; Yumura, M.; Iijima, S. Shape-Engineerable and Highly Densely Packed Single-Walled Carbon Nanotubes and Their Application as Super-Capacitor Electrodes. *Nat. Mater.* **2006**, *5*, 987−994.

(11) Fan, S. S.; Chapline, M. G.; Franklin, N. R.; Tombler, T. W.; Cassell, A. M.; Dai, H. J. Self-Oriented Regular Arrays of Carbon Nanotubes and Their Field Emission Properties. *Science* **1999**, *283*, 512−514.

(12) Milne, W. I.; Teo, K. B. K.; Amaratunga, G. A. J.; Legagneux, P.; Gangloff, L.; Schnell, J. P.; Semet, V.; Binh, V. T.; Groening, O. Carbon Nanotubes as Field Emission Sources. *J. Mater. Chem.* **2004**, *14*, 933−943.

(13) Hinds, B. J.; Chopra, N.; Rantell, T.; Andrews, R.; Gavalas, V.; Bachas, L. G. Aligned Multiwalled Carbon Nanotube Membranes. *Science* **2004**, *303*, 62−65.

(14) Holt, J. K.; Park, H. G.; Wang, Y. M.; Stadermann, M.; Artyukhin, A. B.; Grigoropoulos, C. P.; Noy, A.; Bakajin, O. Fast Mass Transport through Sub-2-Nanometer Carbon Nanotubes. *Science* **2006**, *312*, 1034−1037.

(15) Mi, W. L.; Lin, Y. S.; Li, Y. D. Vertically Aligned Carbon Nanotube Membranes on Macroporous Alumina Supports. *J. Membr. Sci.* **2007**, *304*, 1−7.

(16) Nihei, M.; Kawabata, A.; Awano, Y. Direct Diameter-Controlled Growth of Multiwall Carbon Nanotubes on Nickel-Silicide Layer. *Jpn. J. Appl. Phys.* **2003**, *42*, L721−L723.

(17) Cantoro, M.; Hofmann, S.; Pisana, S.; Scardaci, V.; Parvez, A.; Ducati, C.; Ferrari, A. C.; Blackburn, A. M.; Wang, K. Y.; Robertson, J. Catalytic Chemical Vapor Deposition of Single-Wall Carbon Nanotubes at Low Temperatures. *Nano Lett.* **2006**, *6*, 1107−1112.

(18) Yokoyama, D.; Iwasaki, T.; Ishimaru, K.; Sato, S.; Hyakushima, T.; Nihei, M.; Awano, Y.; Kawarada, H. Electrical Properties of Carbon Nanotubes Grown at a Low Temperature for Use as Interconnects. *Jpn. J. Appl. Phys.* **2008**, *47*, 1985−1990.

(19) Shang, N. G.; Tan, Y. Y.; Stolojan, V.; Papakonstantinou, P.; Silva, S. R. P. High-Rate Low-Temperature Growth of Vertically Aligned Carbon Nanotubes. *Nanotechnology* **2010**, *21*, 505604.

(20) Sugime, H.; Esconjauregui, S.; Yang, J. W.; D'Arsie, L.; Oliver, R. A.; Bhardwaj, S.; Cepek, C.; Robertson, J. Low Temperature Growth of Ultra-High Mass Density Carbon Nanotube Forests on Conductive Supports. *Appl. Phys. Lett.* **2013**, *103*, 073116.

(21) Sugime, H.; Esconjauregui, S.; D'Arsie, L.; Yang, J. W.; Makaryan, T.; Robertson, J. Growth Kinetics and Growth Mechanism of Ultrahigh Mass Density Carbon Nanotube Forests on Conductive Ti/Cu Supports. *ACS Appl. Mater. Interfaces* **2014**, *6*, 15440−15447.

(22) Na, N.; Kim, D. Y.; So, Y. G.; Ikuhara, Y.; Noda, S. Simple and Engineered Process Yielding Carbon Nanotube Arrays with 1.2×10^{13} cm^{-2} Wall Density on Conductive Underlayer at 400 °C. *Carbon* **2015**, *81*, 773−781.

(23) Huang, J. Y.; Chen, S.; Jo, S. H.; Wang, Z.; Han, D. X.; Chen, G.; Dresselhaus, M. S.; Ren, Z. F. Atomic-Scale Imaging of Wall-by-Wall Breakdown and Concurrent Transport Measurements in Multiwall Carbon Nanotubes. *Phys. Rev. Lett.* **2005**, *94*, 236802.

(24) Esconjauregui, S.; Fouquet, M.; Bayer, B. C.; Ducati, C.; Smajda, R.; Hofmann, S.; Robertson, J. Growth of Ultrahigh Density Vertically Aligned Carbon Nanotube Forests for Interconnects. *ACS Nano* **2010**, *4*, 7431−7436.

DOI: 10.1021/acsami.5b04846
ACS Appl. Mater. Interfaces 2015, 7, 16819−16827

(25) Zhong, G. F.; Warner, J. H.; Fouquet, M.; Robertson, A. W.; Chen, B. A.; Robertson, J. Growth of Ultrahigh Density Single-Walled Carbon Nanotube Forests by Improved Catalyst Design. *ACS Nano* **2012**, *6*, 2893−2903.
(26) Delzeit, L.; Nguyen, C. V.; Chen, B.; Stevens, R.; Cassell, A.; Han, J.; Meyyappan, M. Multiwalled Carbon Nanotubes by Chemical Vapor Deposition Using Multilayered Metal Catalysts. *J. Phys. Chem. B* **2002**, *106*, 5629−5635.
(27) Cui, H.; Eres, G.; Howe, J. Y.; Puretkzy, A.; Varela, M.; Geohegan, D. B.; Lowndes, D. H. Growth Behavior of Carbon Nanotubes on Multilayered Metal Catalyst Film in Chemical Vapor Deposition. *Chem. Phys. Lett.* **2003**, *374*, 222−228.
(28) Hata, K.; Futaba, D. N.; Mizuno, K.; Namai, T.; Yumura, M.; Iijima, S. Water-Assisted Highly Efficient Synthesis of Impurity-Free Single-Waited Carbon Nanotubes. *Science* **2004**, *306*, 1362−1364.
(29) Zhong, G. F.; Iwasaki, T.; Honda, K.; Furukawa, Y.; Ohdomari, I.; Kawarada, H. Low Temperature Synthesis of Extremely Dense, and Vertically Aligned Single-Walled Carbon Nanotubes. *Jpn. J. Appl. Phys.* **2005**, *44*, 1558−1561.
(30) Noda, S.; Hasegawa, K.; Sugime, H.; Kakehi, K.; Zhang, Z. Y.; Maruyama, S.; Yamaguchi, Y. Millimeter-Thick Single-Walled Carbon Nanotube Forests: Hidden Role of Catalyst Support. *Jpn. J. Appl. Phys.* **2007**, *46*, L399−L401.
(31) Chakrabarti, S.; Kume, H.; Pan, L. J.; Nagasaka, T.; Nakayama, Y. Number of Walls Controlled Synthesis of Millimeter-Long Vertically Aligned Brushlike Carbon Nanotubes. *J. Phys. Chem. C* **2007**, *111*, 1929−1934.
(32) Ohno, H.; Takagi, D.; Yamada, K.; Chiashi, S.; Tokura, A.; Homma, Y. Growth of Vertically Aligned Single-Walled Carbon Nanotubes on Alumina and Sapphire Substrates. *Jpn. J. Appl. Phys.* **2008**, *47*, 1956−1960.
(33) Sugime, H.; Noda, S. Millimeter-Tall Single-Walled Carbon Nanotube Forests Grown from Ethanol. *Carbon* **2010**, *48*, 2203−2211.
(34) Murakami, Y.; Chiashi, S.; Miyauchi, Y.; Hu, M. H.; Ogura, M.; Okubo, T.; Maruyama, S. Growth of Vertically Aligned Single-Walled Carbon Nanotube Films on Quartz Substrates and Their Optical Anisotropy. *Chem. Phys. Lett.* **2004**, *385*, 298−303.
(35) Christen, H. M.; Puretzky, A. A.; Cui, H.; Belay, K.; Fleming, P. H.; Geohegan, D. B.; Lowndes, D. H. Rapid Growth of Long, Vertically Aligned Carbon Nanotubes through Efficient Catalyst Optimization Using Metal Film Gradients. *Nano Lett.* **2004**, *4*, 1939−1942.
(36) Noda, S.; Sugime, H.; Osawa, T.; Tsuji, Y.; Chiashi, S.; Murakami, Y.; Maruyama, S. A Simple Combinatorial Method to Discover Co-Mo Binary Catalysts That Grow Vertically Aligned Single-Walled Carbon Nanotubes. *Carbon* **2006**, *44*, 1414−1419.
(37) Zhang, L.; Tan, Y. Q.; Resasco, D. E. Controlling the Growth of Vertically Oriented Single-Walled Carbon Nanotubes by Varying the Density of Co-Mo Catalyst Particles. *Chem. Phys. Lett.* **2006**, *422*, 198−203.
(38) Herrera, J. E.; Balzano, L.; Borgna, A.; Alvarez, W. E.; Resasco, D. E. Relationship between the Structure/Composition of Co-Mo Catalysts and Their Ability to Produce Single-Walled Carbon Nanotubes by Co Disproportionation. *J. Catal.* **2001**, *204*, 129−145.
(39) Hu, M. H.; Murakami, Y.; Ogura, M.; Maruyama, S.; Okubo, T. Morphology and Chemical State of Co-Mo Catalysts for Growth of Single-Walled Carbon Nanotubes Vertically Aligned on Quartz Substrates. *J. Catal.* **2004**, *225*, 230−239.
(40) Horibe, M.; Nihei, M.; Kondo, D.; Kawabata, A.; Awano, Y. Carbon Nanotube Growth Technologies Using Tantalum Barrier Layer for Future Ulsis with Cu/Low-K Interconnect Processes. *Jpn. J. Appl. Phys.* **2005**, *44*, 5309−5312.
(41) Nessim, G. D.; Seita, M.; O'Brien, K. P.; Hart, A. J.; Bonaparte, R. K.; Mitchell, R. R.; Thompson, C. V. Low Temperature Synthesis of Vertically Aligned Carbon Nanotubes with Electrical Contact to Metallic Substrates Enabled by Thermal Decomposition of the Carbon Feedstock. *Nano Lett.* **2009**, *9*, 3398−3405.
(42) Kleyna, R.; Mex, H.; Voss, M.; Borgmann, D.; Viscido, L.; Heras, J. M. Modification of MoO_3 Surfaces by Vapour-Deposited Cobalt Atoms. *Surf. Sci.* **1999**, *433*, 723−727.
(43) Werfel, F.; Minni, E. Photoemission-Study of the Electronic-Structure of Mo and Mo Oxides. *J. Phys. C: Solid State Phys.* **1983**, *16*, 6091−6100.
(44) Bayer, B. C.; Zhang, C.; Blume, R.; Yan, F.; Fouquet, M.; Wirth, C. T.; Weatherup, R. S.; Lin, L.; Baehtz, C.; Oliver, R. A.; Knop-Gericke, A.; Schlogl, R.; Hofmann, S.; Robertson, J. In-Situ Study of Growth of Carbon Nanotube Forests on Conductive $CoSi_2$ Support. *J. Appl. Phys.* **2011**, *109*, 114314.
(45) Kawabata, A.; Murakami, T.; Nihei, M.; Yokoyama, N. Growth of Dense, Vertical and Horizontal Graphene and Its Thermal Properties. *Jpn. J. Appl. Phys.* **2013**, *52*, 04CB06.
(46) Eres, G.; Kinkhabwala, A. A.; Cui, H. T.; Geohegan, D. B.; Puretzky, A. A.; Lowndes, D. H. Molecular Beam-Controlled Nucleation and Growth of Vertically Aligned Single-Wall Carbon Nanotube Arrays. *J. Phys. Chem. B* **2005**, *109*, 16684−16694.
(47) Zhong, G.; Hofmann, S.; Yan, F.; Telg, H.; Warner, J. H.; Eder, D.; Thomsen, C.; Milne, W. I.; Robertson, J. Acetylene: A Key Growth Precursor for Single-Walled Carbon Nanotube Forests. *J. Phys. Chem. C* **2009**, *113*, 17321−17325.
(48) Sugime, H.; Noda, S. Cold-Gas Chemical Vapor Deposition to Identify the Key Precursor for Rapidly Growing Vertically-Aligned Single-Wall and Few-Wall Carbon Nanotubes from Pyrolyzed Ethanol. *Carbon* **2012**, *50*, 2953−2960.
(49) Wang, Y. Y.; Luo, Z. Q.; Li, B.; Ho, P. S.; Yao, Z.; Shi, L.; Bryan, E. N.; Nemanich, R. J. Comparison Study of Catalyst Nanoparticle Formation and Carbon Nanotube Growth: Support Effect. *J. Appl. Phys.* **2007**, *101*, 124310.
(50) Dijon, J.; Fournier, A.; Szkutnik, P. D.; Okuno, H.; Jayet, C.; Fayolle, M. Carbon Nanotubes for Interconnects in Future Integrated Circuits: The Challenge of the Density. *Diamond Relat. Mater.* **2010**, *19*, 382−388.
(51) Esconjauregui, S.; Bayer, B. C.; Fouquet, M.; Wirth, C. T.; Yan, F.; Xie, R.; Ducati, C.; Baehtz, C.; Castellarin-Cudia, C.; Bhardwaj, S.; Cepek, C.; Hofmann, S.; Robertson, J. Use of Plasma Treatment to Grow Carbon Nanotube Forests on TiN Substrate. *J. Appl. Phys.* **2011**, *109*, 114312.
(52) Khassin, A. A.; Yurieva, T. M.; Kaichev, V. V.; Bukhtiyarov, V. I.; Budneva, A. A.; Paukshtis, E. A.; Parmon, V. N. Metal-Support Interactions in Cobalt-Aluminum Co-Precipitated Catalysts: Xps and Co Adsorption Studies. *J. Mol. Catal. A: Chem.* **2001**, *175*, 189−204.
(53) Haynes, W. M. *CRC Handbook of Chemisty and Physics*, 95th ed.; CRC Press: Boca Raton, FL, 2014.
(54) Bayer, B. C.; Fouquet, M.; Blume, R.; Wirth, C. T.; Weatherup, R. S.; Ogata, K.; Knop-Gericke, A.; Schlogl, R.; Hofmann, S.; Robertson, J. Co-Catalytic Solid-State Reduction Applied to Carbon Nanotube Growth. *J. Phys. Chem. C* **2012**, *116*, 1107−1113.
(55) Michaelis, F. B.; Weatherup, R. S.; Bayer, B. C.; Bock, M. C. D.; Sugime, H.; Caneva, S.; Robertson, J.; Baumberg, J. J.; Hofmann, S. Co-Catalytic Absorption Layers for Controlled Laser-Induced Chemical Vapor Deposition of Carbon Nanotubes. *ACS Appl. Mater. Interfaces* **2014**, *6*, 4025−4032.
(56) Robertson, J.; Zhong, G. F.; Esconjauregui, C. S.; Bayer, B. C.; Zhang, C.; Fouquet, M.; Hofmann, S. Applications of Carbon Nanotubes Grown by Chemical Vapor Deposition. *Jpn. J. Appl. Phys.* **2012**, *51*, 01AH01.
(57) Esconjauregui, S.; Bhardwaj, S.; Yang, J.; Castellarin-Cudia, C.; Xie, R.; D'Arsie, L.; Makaryan, T.; Sugime, H.; Eslava, S.; Cepek, C.; Robertson, J. Carbon Nanotube Growth on Conductors: Influence of the Support Structure and Catalyst Thickness. *Carbon* **2014**, *73*, 13−24.
(58) Tyson, W. R.; Miller, W. A. Surface Free-Energies of Solid Metals - Estimation from Liquid Surface-Tension Measurements. *Surf. Sci.* **1977**, *62*, 267−276.
(59) Sugime, H.; Noda, S.; Maruyama, S.; Yamaguchi, Y. Multiple "Optimum" Conditions for Co-Mo Catalyzed Growth of Vertically

DOI: 10.1021/acsami.5b04846
ACS Appl. Mater. Interfaces 2015, 7, 16819−16827

Aligned Single-Walled Carbon Nanotube Forests. *Carbon* **2009**, *47*, 234−241.
(60) Yoshida, H.; Takeda, S.; Uchiyama, T.; Kohno, H.; Homma, Y. Atomic-Scale in-Situ Observation of Carbon Nanotube Growth from Solid State Iron Carbide Nanoparticles. *Nano Lett.* **2008**, *8*, 2082−2086.
(61) Chiodarelli, N.; Richard, O.; Bender, H.; Heyns, M.; De Gendt, S.; Groeseneken, G.; Vereecken, P. M. Correlation between Number of Walls and Diameter in Multiwall Carbon Nanotubes Grown by Chemical Vapor Deposition. *Carbon* **2012**, *50*, 1748−1752.

DOI: 10.1021/acsami.5b04846
ACS Appl. Mater. Interfaces 2015, 7, 16819−16827